VOLUME 120, NUMBER 5
FEBRUARY 11, 1998

JOURNAL OF THE AMERICAN CHEMICAL SOCIETY

EXAFS Characterization of the Intermediate X Generated During the Assembly of the *Escherichia coli* Ribonucleotide Reductase R2 Diferric Tyrosyl Radical Cofactor

Pamela J. Riggs-Gelasco,*† Lijin Shu,‡ Shuxian Chen,§ Doug Burdi,† Boi Hanh Huynh,§ Lawrence Que, Jr.,‡ and JoAnne Stubbe†

Contribution from the Chemistry Department, Massachusetts Institute of Technology, 77 Massachusetts Avenue, Cambridge, Massachusetts 02139, Department of Chemistry, Center for Metals in Biocatalysis, University of Minnesota, Minneapolis, Minnesota 55455, and Physics Department, Emory University, Atlanta, Georgia 30322

Received June 3, 1997. Revised Manuscript Received October 24, 1997

Abstract: The assembly of the essential diferric cluster/tyrosyl radical cofactor of the R2 subunit of *Escherichia coli* ribonucleotide reductase from apoR2 with Fe^{2+} and O_2 or diferrous R2 with O_2 has been studied by a variety of rapid kinetic methods. An intermediate **X**, formally an Fe^{3+}/Fe^{4+} diiron cluster, oxidizes tyrosine 122 to the tyrosyl radical concomitant with its own reduction to the diferric cluster generating the R2 cofactor. To characterize the properties of **X**, rapid freeze quench methods have been used in conjunction with Mössbauer, ENDOR, and EPR spectroscopies. These studies are extended here to include rapid freeze quench EXAFS. A short, 2.5 Å Fe−Fe vector and a 1.8 Å Fe−O interaction have been identified in nine independent samples of **X**. These samples have been generated using both wild-type and a mutant protein in which the essential tyrosine has been replaced by phenylalanine (Y122F). The short Fe−Fe interaction is neither present in diferrous or diferric R2 nor in samples of **X** that have aged to decay the intermediate. Several structural models which are consistent with the data are presented.

Introduction

Ribonucleotide reductases (RNRs) catalyze the production of deoxyribonucleotides from ribonucleotides, an essential step in DNA biosynthesis. The aerobic *Escherichia coli* RNR is a diphosphate reductase (eq 1) and is composed of two nonidentical homodimeric subunits: R1 and R2 (nrdA and nrdB gene products). R1 contains the substrate binding domain and the five redox active cysteines required for reduction.[1,2] R2 contains an essential diferric cluster and tyrosyl radical ($Y122^{\bullet}$).[3] The

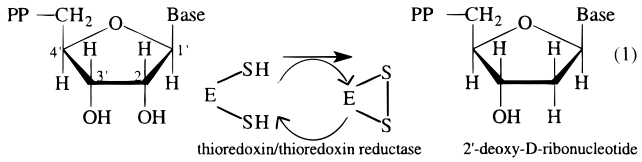

(1)

R2 cofactor is proposed to generate, via long-range coupled electron and proton transfer,[4−6] a thiyl radical on R1 that initiates substrate reduction.[7] Given the importance of the tyrosyl radical, the mechanism by which it is generated from diferrousor apoR2 has been studied using a variety of time-resolved physical biochemical methods.[8−16] Studies reported herein describe the use of rapid freeze quenching methods (RFQ)[17,18] coupled to

† Massachusetts Institute of Technology.
‡ University of Minnesota.
§ Emory University.

S0002-7863(97)01823-4 CCC: $15.00
Published on Web 01/27/1998

both EXAFS (extended X-ray absorption fine structure) and Mössbauer spectroscopy as part of an effort to characterize structurally the diiron intermediate **X**, which is thought to generate directly Y122• during activation of RNR.

Studies of Atkin et al. in 1973 were the first to reveal that this diferric cluster and tyrosyl radical cofactor could be efficiently self-assembled by incubation of apoR2 with Fe^{2+}, O_2, and reductant.[8] More recently, the stoichiometry of this reaction has been determined by several research groups (eq 2).[19−21]

$$\text{Y122}-\text{R2} + 2\text{Fe}^{2+} + \text{O}_2 + \text{e}^- + \text{H}^+ \rightarrow \text{Y122}^\bullet-\text{R2} + \text{Fe}^{3+}(\mu\text{-O})\text{Fe}^{3+} + \text{H}_2\text{O} \quad (2)$$

In vitro, the extra electron required for the $4e^-$ reduction of O_2 to H_2O can be provided by Fe^{2+} or by an exogenous reductant such as ascorbate.[9]

The ability to self-assemble the active cofactor from both apo- and diferrous R2 has allowed the study of the assembly process by various techniques such as Mössbauer, ENDOR, EPR, stopped flow absorption,[8−16] and resonance Raman spectroscopies.[22] In 1994, Bollinger et al. reported a detailed kinetic investigation of the reaction of apoR2 with Fe^{2+} and O_2 that revealed an intermediate, designated **X**, which is kinetically competent in the oxidation of Y122 to Y122•.[11−13] More recently, Tong et al. demonstrated that the same intermediate is formed during the reaction of diferrous R2 with O_2.[16,23] Stopped flow absorption and rapid freeze quenching methods have indicated that **X** has a broad absorbance maximum at 365 nm, is EPR active, and generates Y122• at 4 °C with a rate constant of $\sim 1\ s^{-1}$. Similar studies have been carried out with Y122F−R2, a mutant in which the essential tyrosine residue is replaced with a less oxidizable phenylalanine, in an effort to increase the amount and lifetime of **X**. EPR spectroscopy demonstrated that **X** generated from either wild-type R2 (WT-R2) or Y122F−R2 exhibits a nearly isotropic $S = {}^1/_2$ signal at $g = 2$ that is broadened by carrying out the reconstitution in $^{17}O_2$, $H_2{}^{17}O$, and ^{57}Fe.[9,11] Mössbauer spectroscopy revealed that **X** is composed of two inequivalent Fe sites.[13] Using hyperfine values obtained from analysis of the ^{57}Fe Q-band ENDOR spectrum of **X**, the Mössbauer isomer shifts have been recalculated to be 0.56 and 0.26 mm/s.[14] The former is indicative of high-spin ferric ion, while the latter is intermediate between those observed for high-spin Fe^{3+} and Fe^{4+} in both model complexes and proteins.[14] The smaller isomer shift and the significant hyperfine anisotropy of the latter site established by ENDOR spectroscopy have led to the latest formulation of **X** as an Fe^{3+}/Fe^{4+} pair with significant spin delocalization onto the oxygen ligands.[14] ^1H and ^{17}O ENDOR studies of **X** generated from Y122F−R2 have also demonstrated that it contains two oxygens from O_2: one as a μ-oxo bridge and a second as H_2O or as a positionally disordered OH^- that can exchange with solvent.[24,25] In addition to providing a means to structurally characterize this reactive intermediate, the use of the discontinuous RFQ Mössbauer and EPR methods has allowed independent confirmation of the rate constants obtained with the continuous method of stopped flow absorption spectroscopy.[11−14] Finally, resonance Raman studies of the reconstitution of apo-Y122F−R2 with Fe and $^{18}O_2$ suggest that the μ-oxo bridge in diferric R2 is derived from O_2 gas.[22]

Formulation of a detailed structure to **X** has been aided by the availability of the three-dimensional crystal structures of both diferrous R2[26] and met-diferric R2 (met = Y122• is reduced).[4,27] Scheme 1 summarizes the crystallographic details of the dinuclear iron site in both oxidation states. In the diferrous state, the two four-coordinate iron atoms are separated by 3.9 Å, a consequence of the bis-carboxylato (Glu238 and Glu115) bridging.[26] The Fe coordination numbers for the diferrous state differ from those suggested by analysis of recent MCD data,[28] where one of the iron atoms is proposed to be 5 coordinate.[29] The reason for this discrepancy is presently not understood.

The crystal structure[4,27] of μ-oxo-bridged diferric R2 indicates that each iron is hexacoordinate with an Fe−Fe distance of 3.3 Å.[30] The crystallographic data indicate that the conversion of the diferrous to diferric cluster is accompanied by reorganization of two of the carboxylate ligands. Because of carboxylate shifts, the bridging Glu238 becomes a terminal monodentate ligand and Asp84 changes to a terminal bidentate ligand. A water molecule on each iron completes the coordination spheres. The

(1) Stubbe, J. *Adv. Enzymol. Relat. Areas Mol. Biol.* **1990**, *63*, 349−417.
(2) Reichard, P. *Science* **1993**, *260*, 1773−1777.
(3) Larsson, A.; Sjöberg, B.-M. *EMBO J.* **1986**, *5*, 2037−2040.
(4) Nordlund, P.; Eklund, H. *J. Mol. Biol.* **1993**, *232*, 123−164.
(5) Stubbe, J. *Nature* **1990**, *370*, 502.
(6) Ekberg, M.; Sahlin, M.; Eriksson, M.; Sjöberg, B.-M. *J. Biol. Chem.* **1996**, *34*, 20655−20659.
(7) Stubbe, J. *J. Biol. Chem.* **1990**, *265*, 5329−5332.
(8) Atkin, C. L.; Thelander, L.; Reichard, P.; Lang, G. *J. Biol. Chem.* **1973**, *248*, 7464−7472.
(9) Bollinger, J. M. J.; Edmondson, D. E.; Huynh, B. H.; Filley, J.; Norton, J. R.; Stubbe, J. *Science* **1991**, *253*, 292−298.
(10) Bollinger, J. M. J.; Stubbe, J.; Huynh, B. H.; Edmondson, D. E. *J. Am. Chem. Soc.* **1991**, *113*, 6289−6291.
(11) Bollinger, J. M. J.; Tong, W. H.; Ravi, N.; Huynh, B. H.; Edmondson, D. E.; Stubbe, J. *J. Am. Chem. Soc.* **1994**, *116*, 8024−8032.
(12) Bollinger, J. M. J.; Tong, W. H.; Ravi, N.; Huynh, B. H.; Edmonson, D. E.; Stubbe, J. *J. Am. Chem. Soc.* **1994**, *116*, 8015−8023.
(13) Ravi, N.; Bollinger, J. M. J.; Huynh, B. H.; Stubbe, J.; Edmondson, D. E. *J. Am. Chem. Soc.* **1994**, *116*, 8007−8014.
(14) Sturgeon, B. E.; Burdi, D.; Chen, S.; Huynh, B. H.; Edmondson, D. E.; Stubbe, J.; Hoffman, B. M. *J. Am. Chem. Soc.* **1996**, *118*, 7551−7557.
(15) Burdi, D.; Sturgeon, B. E.; Tong, W. H.; Stubbe, J.; Hoffman, B. M. *J. Am. Chem. Soc.* **1996**, *118*, 281−282.
(16) Tong, W. H.; Chen, S.; Lloyd, S.; Edmondson, D.; Huynh, B. H.; Stubbe, J. *J. Am. Chem. Soc.* **1996**, *118*, 2107−2108.
(17) Ballou, D. P.; Palmer, G. *Anal. Chem.* **1974**, *46*, 1248.
(18) Bollinger, J. M.; Tong, W. H.; Ravi, N.; Huynh, B. H.; Edmondson, D. E.; Stubbe, J. In *Methods in Enzymology*; Klinman, J., Ed.; Academic Press: New York, 1995; Vol. 258.
(19) Bollinger, J. M., Ph.D. Thesis, Massachusetts Institute of Technology, 1993.
(20) Lynch, J. B.; Juarez-Garcia, C.; Münck, E.; Que, L., Jr. *J. Biol. Chem.* **1989**, *264*, 8091−8096.
(21) Ochiai, E.; Mann, G. J.; Gräslund, A.; Thelander, L. *J. Biol. Chem.* **1990**, *265*, 15758−15761.
(22) Ling, J.; Sahlin, M.; Sjöberg, B. M.; Loehr, T. M.; Sanders, L. J. *J. Biol. Chem.* **1994**, *269*, 5595−5601.
(23) Tong, W. H., Ph.D. Thesis, Massachusetts Institute of Technology, 1996.
(24) Willems, J.-P.; Lee, H. I.; Burdi, D.; Doan, P. E.; Stubbe, J.; Hoffman, B. M. *J. Am. Chem. Soc.* **1997**, *119*, 9816−9824.
(25) Burdi, D.; Willems, J.-P.; Stubbe, J.; Hoffman, B. Manuscript in preparation.
(26) Logan, D. T.; Su, X.-D.; Åberg, A.; Regnstrom, K.; Hajdu, J.; Eklund, H.; Nordlund, P. *Structure* **1996**, *4*, 1053−1064.
(27) Nordlund, P.; Sjöberg, B. M.; Eklund, H. *Nature (London)* **1990**, *345*, 593−598.
(28) Pulver, S. C.; Tong, W. H.; Bollinger, J. M.; Stubbe, J.; Solomon, E. *J. Am. Chem. Soc.* **1995**, *117*, 12644−12678.
(29) Diferrous R2 for the MCD study was prepared either by incubation of apoR2 with Fe^{2+} or by reduction of diferric R2 with dithionite. The samples for crystallization were prepared either by photoreduction of met-R2 in the X-ray beam (100 K structure, 1.7 Å resolution) or by chemical reduction with a 3% dithionite solution (room-temperature structure, 2.1 Å resolution).
(30) The crystallization was carried out at pH 6 in the presence of ethyl mercurithiosalicylate, and the consequences of these conditions on the coordination of the iron environment is presently unknown.

Scheme 1

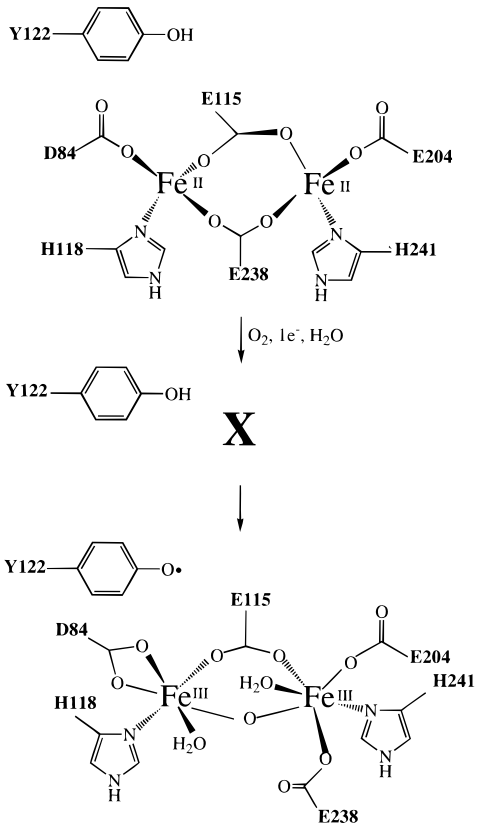

essential tyrosyl radical is 5.3 Å from the nearest Fe and is buried 10 Å from the surface of the protein.

The unusual and unprecedented spectroscopic properties of **X** begs a comparison to the few relevant model systems and to the protein methane monooxygenase (MMO) which catalyzes the formation of methanol from methane with a high-valent iron cluster. Compound **Q** is proposed to be the kinetically competent intermediate in this oxidation, and it consists of two antiferromagnetically coupled Fe(IV) atoms, on the basis of its Mössbauer isomer shifts of $\delta = 0.14-0.21$.[31,32] Whereas diamagnetic **Q** undergoes two-electron reduction to afford diferric MMO and methanol, the paramagnetic **X** carries out one-electron chemistry in the oxidation of tyrosine to the tyrosyl radical. The crystallographic similarities between active sites of diferrous R2 and MMO[26,33] have prompted several groups to speculate that the chemistry of dioxygen activation in these two enzymes proceeds through a common mechanistic framework.[34,35]

Recently Que and co-workers, using the ligands tris(2-pyridylmethyl)amine (TPA) and its ring-methylated derivatives, have generated a family of bis(μ-oxo)diiron compounds that may serve as models for the intermediate **X** and/or compound **Q**.[34,36−39] Of these synthetic complexes, $[Fe^{3+}{}_2(O)_2(6\text{-Me}_3\text{-TPA})_2](ClO_4)_2$ is crystallographically characterized and exhibits an Fe−Fe distance of 2.71 Å and an unusually small Fe−μ-O−Fe angle of 92.5°. Related Fe^{3+}/Fe^{4+} complexes have been generated by the reaction of diiron(III) precursors with H_2O_2. EXAFS studies indicate that the resulting products have Fe−Fe distances of 2.9−3.0 Å, consistent with the proposed $Fe_2(\mu\text{-}O)_2$ core. The high-spin Fe^{3+}/Fe^{4+} 6-Me-TPA compound (6-Me-TPA = *N*-(6-methyl-2-pyridylmethyl)-*N*,*N*-bis(2-pyridylmethyl)amine)[38] (**1**) in particular exhibits an EPR spectrum that is virtually identical with that of intermediate **X**, though the properties of the putative Fe^{4+} site ($\delta = 0.08$ mm/s; A1, A2, A3 = 20, 36.5, 36.5 MHz) differ somewhat from those of **X** ($\delta = 0.26$ mm/s; A1, A2, A3 = 27.5, 36.8, 36.8 MHz).[14] These spectroscopic similarities suggest that **X** may have an $Fe_2(\mu\text{-}O)_2$ core, the presence of which would be manifested by the appearance of a short Fe−Fe distance in the EXAFS spectrum by analogy to those of the model complexes.

We have therefore extended the series of rapid freeze quench spectroscopic studies of **X** to include RFQ EXAFS. Although the use of RFQ methods in conjunction with X-ray absorption spectroscopy has been reported previously, its use has been quite limited.[40−43] For **X**, the composition of the sample can be determined prior to and after the XAS experiment with Mössbauer spectroscopy, eliminating some of the uncertainty associated with data analysis of a heterogeneous sample. In addition, a high percent composition of **X** has been generated in the presence of diferrous R2, rather than diferric R2, since the diferrous Fe−Fe vector is less likely to interfere with the identification of an Fe−Fe interaction of **X**.[44] The results described herein demonstrate that the intermediate **X** in the assembly of the essential cofactor of *E. coli* RNR has a novel Fe−Fe interaction of 2.5 Å and at least one μ-oxo bridge. These results provide an essential piece to the puzzle with a goal of assigning a detailed structure to **X**.

Experimental Section

Sample Preparation. pTB2 and pTB2−Y122F plasmids[12] were transformed into the *E. coli* host strain BL21(DE3) (Novagen). The method of protein purification has been described elsewhere.[12] The overexpressed WT-R2 had a specific activity of 7000 U/mg (Units (U) = nmol/min) using a spectrophotometric assay as previously described.[45] A modification of the method of Atkin et al. was used to prepare apo enzyme.[8] WT-R2 (30 mg/mL) was incubated for 15 min with 30 mM NH_2OH to reduce the tyrosyl radical. The resulting metR2 was then dialyzed for 5−6 h against a solution of 50 mM lithium 8-hydroxyquinoline-5-sulfonate in 1 M imidazole hydrochloride (pH 7, 4 °C). The Fe−chelator complex was separated from the protein by Sephadex G-50 (Sigma) chromatography in 100 mM Hepes (pH 7.7, 4 °C). The Fe^{2+}/protein ratio of the apo protein was less than 0.1 and was determined by colorimetric assay using the iron chelator

(31) Feig, A. L.; Lippard, S. J. *Chem. Rev.* **1994**, *94*, 759−805 and references therein.
(32) Wallar, B.; Lipscomb, J. D. *Chem. Rev.* **1996**, *96*, 2625−2657 and references therein.
(33) Rosenzweig, A. C.; Nordlund, P.; Takahara, P. M.; Frederick, C. A.; Lippard, S. J. *Chem. Biol.* **1995**, *2*, 409−418.
(34) Que, L., Jr.; Dong, Y. *Acc. Chem. Res.* **1996**, *29*, 190−196.
(35) Nordlund, P.; Eklund, H. *Curr. Opin. Struct. Biol.* **1995**, *5*, 758−766.
(36) Zang, Y.; Dong, Y.; Que, L., Jr.; Kauffmann, K.; Münck, E. *J. Am. Chem. Soc.* **1995**, *117*, 1169−1170.
(37) Dong, Y.; Fujii, H.; Hendrich, M. P.; Leising, R. A.; Pan, G.; Randall, C. R.; Wilkinson, E. C.; Zang, Y.; Que, L., Jr.; Fox, B.; Kauffman, K.; Münck, E. *J. Am. Chem. Soc.* **1995**, *117*, 2778−2792.
(38) Dong, Y.; Que, L., Jr.; Kauffman, K.; Munck, E. *J. Am. Chem. Soc.* **1995**, *117*, 11377−11378.
(39) Kim, C.; Dong, Y.; Que, L., Jr. *J. Am. Chem. Soc.* **1997**, *119*, 3635−3636.
(40) George, G. N.; Bray, R. C.; Cramer, S. P. *Biochem. Soc. Trans.* **1986**, *14*, 651−652.
(41) Saigo, S.; Sone, N.; Nagamura, T.; Oyanagi, H.; Iizuka, T.; Kusunoki, M.; Matsushita, T. In *Biophysics and Synchrotron Radiation*; Bianconi, A., Castellano, A. C., Eds.; Springer-Verlag: New York, 1986; pp 131−135.
(42) Saigo, S.; Hashimoto, H.; Shibayama, N.; Nomura, M.; Nagamura, T. *Biochim. Biophys. Acta* **1993**, *1202*, 99−106.
(43) Shu, L.; Nesheim, J. C.; Kaufmann, K.; Münck, E.; Lipscomb, J. D.; Que, L., Jr. *Science* **1997**, *275*, 515−518.
(44) Unpublished results of L. Que and this work demonstrate the lack of a detectable Fe−Fe vector in diferrous R2.
(45) Salowe, S. P.; Stubbe, J. *J. Bacteriol.* **1986**, *165*, 363−366.

Table 1. Reaction Conditions and Results to Mössbauer Fitting Analysis[a]

	sample[b]	$[R2]_f$ (mM)	Fe^{2+} (equiv)	rxn time	ferrous (%)[a]	X (%)	diferric (%)
1[c]	preload WT **X**	0.50	3.5	158 ms	30	60	8
2	preload WT **X**	0.50	3.5	158 ms	32	54	7
3	preload WT **X**	0.50	3.5	158 ms	39	53	8
4	preload WT **X**	0.50	4.0	110 ms	22	58	15
5	preload WT **X**	0.50	3.5	110 ms	20	66	10
6	preload Y122F **X**	0.50	3.5	195 ms	35	63	2
7	apo-Y122F **X**	0.75	3.0	350 ms	25	68	4
8	apo-Y122F **X**	0.50	3.0	350 ms	35	60	5
9	apo-Y122F **X**	0.50	3.0	442 ms	27	62	8
10	preload WT diferrous	1.5	2.3	28 ms	92	0	0
11	as-isolated WT diferric	1.8					
12	as-isolated Y122F diferric	1.8					
13	preload WT	1.0	3.5	1 min	10	10	78
7w[d]	apo-Y122F **X** after warming	1.5	3.0		4	0	92

[a] Uncertainties in quantitation are estimated to be ±1−2% and result from imperfect reference spectra and from differences in spectral resolution. Percentages may not add to 100% due to the presence of unknown species that cannot be quantitated. [b] Preload samples: both syringes were in 100 mM Hepes, pH 7.6; protein syringe is anaerobic. Apo samples: protein was in 100 mM Hepes, pH 7.7 and Fe^{2+} was in 5 mN H_2SO_4; both sides were O_2 saturated. All samples of **X** except for sample 4 were generated in the presence of 5 mM sodium ascorbate (initial). [c] The data for this sample was collected at NSLS, beamline X-9 at 40 K. All other data were collected at 10 K on beamline 7−3 at SSRL. [d] Composition determined after XAS data acquisition.

ferrozine as previously described.[46−48] A solution of $^{57}Fe^{2+}$ was prepared from $^{57}Fe^0$ (Advanced Materials and Technology (nuggets) or Isotec (fine dust); >95%) as described by Sturgeon et al.[14] or by incubating $^{57}Fe^0$ dust at ambient temperature in 1.25 N H_2SO_4 inside an anaerobic box for 1 week. The solution was diluted with O_2-free water to bring the final H^+ concentration to <10 mM and the Fe^{2+} concentration to 15 mM.[14] Mössbauer spectroscopy was used to verify the lack of any undissolved metallic iron in the solutions used to generate the XAS samples.

Preparation of X by RFQ Methods. The experimental setup and description of the sample holder used to generate rapid freeze quenched Mössbauer samples has been previously described.[13,18] For the EXAFS experiments, the sample holder was modified (Scheme S1, Supporting Information). A hole was cut into the bottom face of the delrin sample cup, and a Mylar film was adhered to the inside of the cup forming a window for the X-ray beam. In this way, Mössbauer spectra were collected on samples prior to and following the XAS experiments. An Update Instruments Drive Ram assembly activated by a model 715 computer controller was used to generate all freeze-quenched samples as previously described.[18]

Either apoR2 or anaerobic diferrous R2 were used in the assembly reactions in this study (hereafter referred to as "apo reconstitution" and "preload assembly", respectively[49]). To prepare the preload samples, 3−4 equiv of $^{57}Fe^{2+}$ in an anaerobic solution of 2.5 mM H_2SO_4 was neutralized with excess buffer, added dropwise with stirring to anaerobic 1 mM apoR2 (WT or Y122F−R2) in a glovebox, and loaded into an airtight syringe (Update Instruments). Specific protein concentrations, Fe^{2+}/R2 ratios, and reaction times are given for each sample studied in Table 1. A detachable bowl (Update Instruments) was used to surround the syringe barrels with an ice bath to maintain the reactions at 5 °C. The reaction was triggered by shooting 250 μL of the anaerobic diferrous R2 (with and without 5 mM ascorbate) against an equal volume of oxygen saturated (∼1.6 mM at 5 °C[50]) 100 mM Hepes, pH 7.6. For reconstitution starting with apo enzyme, a solution containing Y122F−R2 (1.5 mM), 5 mM ascorbate, and 1.6 mM O_2 was rapidly mixed with 3 equiv of $^{57}Fe^{2+}$ in 2.5 mM H_2SO_4. Reaction times are given in Table 1.

Preparation of Control Samples. In addition to the study of **X** by EXAFS, four control samples were prepared.

(1) RFQ−diferrous WT-R2: Anaerobic apoWT-R2 (1.5 mM) and 2.3 equiv of $^{57}Fe^{2+}$ in anaerobic 2.5 mM H_2SO_4 were combined in a glovebox and loaded into two airtight syringes. Using the shortest timing loop, these solutions (250 μL each) were rapidly mixed and quenched at 28 ms. Since this sample was made with $^{57}Fe^{2+}$, $^{57}Fe^0$ contaminants were ruled out as giving rise to the 2.5 Å Fe−Fe vector found in the **X** samples.

(2) Y122F diferric R2 and WT diferric R2: WT or Y122F−R2 (1.75 mM in 100 mM Tris (pH 7.6) with 10% glycerol as a cryoprotectant) was loaded into a dual Mössbauer/EXAFS cell and rapidly frozen in liquid nitrogen.

(3) Conversion of **X** to diferric R2 after EXAFS data collection: A RFQ sample of **X** prepared from Y122F−R2 (sample 7, Table 1) was warmed to room temperature by removing the sample from the liquid He cryostat and incubating at room temperature until all ice had melted. After the sample turned the expected green color, the cell was reimmersed in liquid nitrogen and another EXAFS spectrum was collected.

(4) RFQ−diferric WT-R2: To demonstrate that EXAFS features assigned to **X** decay with time, anaerobic diferrous WT-R2 was allowed to react with oxygenated Hepes for 1 min before quenching (Table 1, sample 13), resulting in a sample that was 10% **X**, 10% diferrous, and 78% diferric enzyme.

Mössbauer Analysis. Mössbauer spectra were recorded at 4.2 K with a 50 mT magnetic field applied parallel to the γ beam as previously described.[13] The spectrometer was equipped with a Janis 8DT variable-temperature cryostat. Quantitations of **X**, diferrous R2, diferric R2, and any other Fe species in the XAS samples were determined using reference Mössbauer spectra.[14,18] Mössbauer spectra were collected before and after the XAS data collection.

XAS Data Collection. XAS data were collected using synchrotron radiation from either the National Synchrotron Light Source (NSLS) beamline X-9 or the Stanford Synchrotron Radiation Laboratory (SSRL) beamline 7-3. At NSLS, samples were maintained at 40 K using a Displex cryostat; a Si(111) double-crystal monochromator was used, and a nickel-plated harmonic rejection mirror allowed the use of a fully tuned X-ray beam. At SSRL, samples were maintained at 10 K using an Oxford instruments continuous flow liquid He cryostat; a Si(220) double-crystal monochromator was used, and harmonic rejection was achieved by detuning the maximum incident intensity of the beam by 50%. At both facilities, a Canberra 13 element solid-state detector was used to detect Fe Kα fluorescence. The thickness of the sample precluded the simultaneous measurement of a calibration foil. Energy calibration scans using an Fe foil were measured prior to and following the sets of EXAFS scans for the samples. Scans were defined with 5−8 eV spacing in the preedge region, a 0.5 eV spacing in the edge

(46) Stookey, L. L. *Anal. Chem.* **1970**, *42*, 779−781.
(47) Salowe, S. P., Ph.D. Thesis, University of Wisconsin, 1987.
(48) Massey, V. *J. Biol. Chem.* **1957**, *229*, 763−770.
(49) The term preload was introduced in ref 16 to indicate an assembly reaction starting with the iron(II) already bound to the protein. In the preload assembly reaction, a conformational change that occurs upon binding of iron is bypassed, resulting in an increased rate constant for the formation of **X** (60−80 s^{-1} instead of 8 s^{-1} for apo reconstitutions). The formation of tyrosyl radical occurs with the same rate constant (1 s^{-1}) in both types of assembly reactions.
(50) Hitchman, M. L. *Measurement of Dissolved Oxygen*; Wiley: New York, 1978.

region, and 0.05 Å^{-1} spacing in the EXAFS region (2−14 Å^{-1}, k^3 weighted collection time). Reported EXAFS spectra of the intermediate are the average of 12−24 individual scans. The ferric controls are the average of six individual scans, and the ferrous control spectrum is an average of eight scans. The total incident count rate was kept in the linear range of the detector (<40 000 at NSLS and <90 000 at SSRL) to minimize deadtime distortion in the data. Typical fluorescence counts at 8000 eV for the intermediate samples were 3000−4000 Hz at SSRL. The background Fe fluorescence measured with and without an empty sample cup was ≤5% of the windowed count rates.

Data Analysis. Upon excitation of a 1s (for K edges) core electron to the continuum, a photoelectron wave generated at the absorbing Fe atom passes through space until a neighboring scattering atom deflects the wave back toward the direction of the absorber. The resulting interference between the outgoing and back-scattered wave results in the modulation of the X-ray absorption coefficient as a function of energy. The EXAFS fitting protocols used here have been described elsewhere.[51] A smooth polynomial background was subtracted from the raw data, and the data were converted to k space (eq 3) where k is the photoelectron wave vector defined by eq 4:

$$\chi(k) = \sum \frac{N_s A_s(k) S}{k R_{as}^2} \exp(-2k^2\sigma_{as}^2) \exp(-2R_{as}/\lambda) \sin(2kR_{as} + \phi_{as}(k)) \quad (3)$$

$$2\pi/\lambda = k = \sqrt{2m_e(E - E_0)/\hbar^2} \quad (4)$$

E_0 is the threshold energy for excitation of a 1s electron to the continuum, and m_e is the mass of the electron. Initially, E_0 was defined to be 7130 eV. The amplitude of the wave function depends on the number of scatterers N_s at distance R_{as} and scales by $1/R_{as}^2$; the amplitude is also exponentially damped by a function of λ, the mean-free path of the photoelectron, and a function of σ_{as}, the mean-square deviation in R_{as}. The back-scattering amplitude, $A_s(k)$, is a function of scatterer type and $\phi_{as}(k)$ is the phase shift that the photoelectron undergoes as it passes through the potentials of the absorber twice and the scatterer once.

Quantitative curve fitting to eq 3 by supplying theoretical or empirical functions for $A_s(k)$ and $\phi_{as}(k)$ yields absorber−scatterer distance information R_{as}, σ_{as}, and N_s. In this work, curved wave theoretical phase and amplitude functions were provided in the program FEFF (version 3.25 for single scattering).[52,53] The theoretical amplitude function was scaled by using a value of 0.9 for S (eq 3). The parameter ΔE_0 was assigned to a fixed value of 10 eV on the basis of previous model work where this value was found to give correct metal−metal distances to the nearest 0.02 Å.[54] When varied for the Fe−Fe shell, ΔE_0 refined to 2−10 eV. A program based on FABM[55] (fine adjustment based on models) which uses calculated phase and amplitude functions using McKale curved wave formalism[56] was also used to independently verify the fitting results. In these latter fits, the amplitude scale factor and the value of ΔE_0 were abstracted from the crystallographically characterized model $[Fe_2^{III}(O)(OH)(6\text{-}Me_3\text{-}TPA)_2](ClO_4)_3$.[57]

Frequency deconvolution using Fourier transform methods gives a phase-shifted radial distribution function in anstrom space. The interactions of interest can then be back transformed to give the Fourier-filtered data, resulting in the removal of high- and low-frequency noise. Data in this work were fit with and without Fourier filtering with equivalent results. Goodness of fit, F, was defined by eq 5:

$$F = [\sum k^6(\chi_{obsd} - \chi_{calcd})^2/N]^{1/2} \quad (5)$$

where N is the number of points in the EXAFS spectrum. As the F value generally improves (becomes smaller) by adding more variables (i.e., shells of scatterers), we also made use of a statistic ϵ',[51,58] which scales the F value according to eq 6:

$$\epsilon' = F^2/\nu \quad (6)$$

where $\nu = N_{PTS} - \rho$. N_{PTS} is the number of degrees of freedom given by $N_{PTS} = 2\Delta k\Delta R/\pi$.[59] ρ is the number of variable parameters in each fit (R and σ for each shell).

Results

Quantitation of Relative Amounts of Diiron Species in the X Samples by Mössbauer Analysis. The kinetics of reconstitution of the active iron center of R2 are such that **X** can never be present as the only iron-containing species. Previous XAS studies have revealed that the 3.9 Å Fe−Fe interaction[26] for diferrous R2 is not observable in the EXAFS[44] while the Fe−Fe vector in diferric R2 is quite prominent at 3.22 Å.[55,60] The potential complications arising from the presence of diferric cluster in the data analysis suggested that samples should be prepared at early quenching times, such that diferrous R2 and **X** are the primary components. To permit collection of Mössbauer and EXAFS spectra on the same sample, the RFQ Mössbauer sample cell[13,18] was redesigned (Scheme 1S, Supporting Information). In this way, the relative amounts of each type of diiron cluster could be established using Mössbauer spectroscopy prior to and after XAS data acquisition. Table 1 summarizes the reaction conditions and sample compositions as determined by Mössbauer analysis.[23] Five samples of **X** generated with WT-R2 (Table 1, samples 1−5) and four samples of **X** generated with Y122F−R2 (Table 1, samples 6−9) have been examined using XAS. After the XAS experiment, the Mössbauer spectra were recollected with virtually identical results (data not shown).

XANES. RFQ ^{57}Fe ENDOR studies indicate that **X** contains an anisotropic Fe, consistent with Fe^{4+}. However, the Mössbauer isomer shift of this Fe is intermediate between the values for Fe^{3+} and Fe^{4+} previously determined on available model systems.[14] Since the position of the rising edge of the X-ray absorption spectrum can be indicative of absorber oxidation state, the X-ray absorption edges of the **X** samples were compared to those of diferrous and diferric R2. Figure 1A shows that the edge energy of **X** (Table 1, sample 3) is intermediate between the diferrous and diferric forms of R2 (Table 1, samples 10 and 11, respectively). This is not surprising since the large Fe^{2+} contents of the heterogeneous **X** samples skew the spectra to low energy thus making it difficult to ascertain if **X** contains Fe^{4+}. By using linear combinations of normalized diferrous (sample 10) and diferric (sample 11) XANES spectra, however, we verified that **X** is minimally a diferric cluster. If **X** is modeled as a diferric cluster, the authentic diferric R2 and diferrous R2 spectra can be combined in a linear combination of the appropriate ratio to reflect the composition of a given **X** sample (for example, the linear combination of sample 3 would be 0.39(ferrous) + 0.61(ferric)). The resulting linear combination spectra are identical in energy to the given **X** edge. Only for samples 4 and 5, which

(51) Riggs-Gelasco, P. J.; Mei, R.; Yocum, C. F.; Penner-Hahn, J. E. *J. Am. Chem. Soc.* **1996**, *118*, 2387−2399.
(52) Rehr, J. J.; Albers, R. C. *Phys. Rev.* **1990**, *B41*, 8139.
(53) Rehr, J. J.; de Leon, J. M.; Zabinsky, S. I.; Albers, R. C. *J. Am. Chem. Soc.* **1991**, *113*, 5135−5140.
(54) Riggs-Gelasco, P. J., Ph.D. Thesis, University of Michigan, 1995.
(55) Scarrow, R. C.; Maroney, M. J.; Palmer, S. M.; Que, L., Jr.; Roe, A. L.; Salowe, S. P.; Stubbe, J. *J. Am. Chem. Soc.* **1987**, *109*, 7857−7864.
(56) McKale, A. G.; Veal, B. W.; Paulikas, A. P.; Chan, S.-K.; Knapp, G. S. *J. Am. Chem. Soc.* **1988**, *110*, 3763−3768.
(57) Shu, L.; Liu, Y.; Lipscomb, J. D.; Que, L., Jr. *J. Biol. Inorg. Chem.* **1996**, *1*, 297−304.
(58) Riggs-Gelasco, P. J.; Stemmler, T. L.; Penner-Hahn, J. E. *Coord. Chem. Rev.* **1996**, *144*, 245−286.
(59) Lytle, F. W.; Sayers, D. E.; Stern, E. A. *Phys. B.* **1989**, *158*, 701−722.
(60) Scarrow, R. C.; Maroney, M. J.; Palmer, S. M.; Que, L., Jr.; Salowe, S. P.; Stubbe, J. *J. Am. Chem. Soc.* **1986**, *108*, 6832−6834.

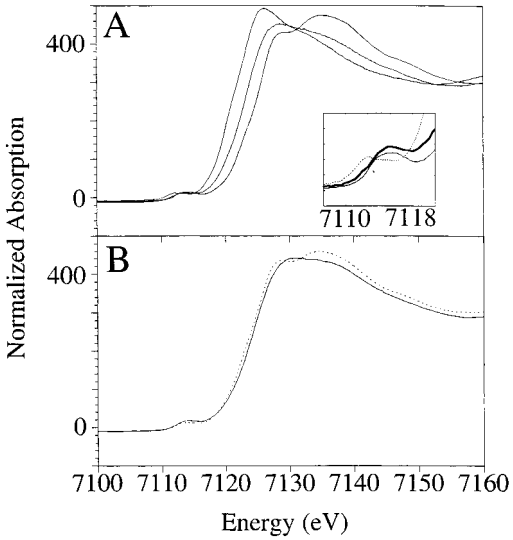

Figure 1. Top frame: normalized XANES spectra (from lowest energy to highest) of diferrous R2, **X** (sample 3), and diferric R2. Inset: 1s → 3d transition for diferrous R2 (dashed line), diferric R2 (solid line), and **X** (sample 3; bold line). Bottom frame: linear combination of the XANES spectra of diferrous and diferric R2, 0.22(ferrous) + 0.78-(ferric) (dashed line). The edge spectrum of **X** (sample 4, 22% diferrous) is only slightly higher in energy (solid line).

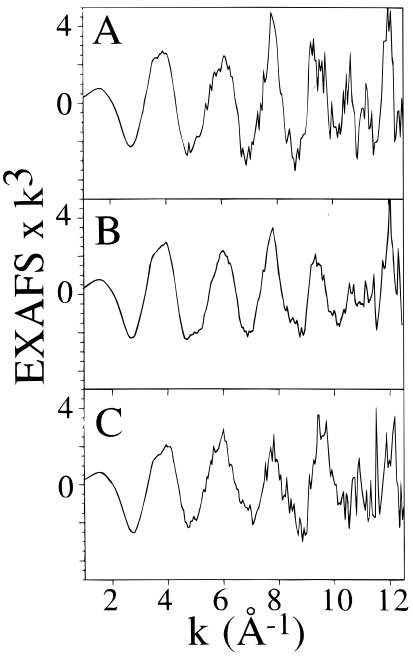

Figure 2. Raw EXAFS data: (A) representative WT preload data set (sample 1); (B) average of 5 WT **X** data sets (samples 1−5); (C) representative apo-Y122F data set (sample 7).

have the lowest Fe^{2+} content, are the authentic **X** spectra slightly higher in energy than the corresponding linear combination spectra (see Figure 1B). These results confirm that **X** is minimally a diferric cluster, but do not establish or refute the presence of Fe^{4+}.[61]

2.5 Å Feature. A primary goal of this work was to identify the Fe−Fe distance in intermediate **X**. Figure 2 shows the raw k^3-weighted EXAFS data of a single WT data set of **X** and the average of the five WT **X** samples (panels A and B, respectively). The raw EXAFS data of **X** does in fact indicate the

(61) The differing shapes of the linear combination spectra and the **X** spectra also verify the presence of a unique species differing from diferrous and diferric R2 in the **X** samples.

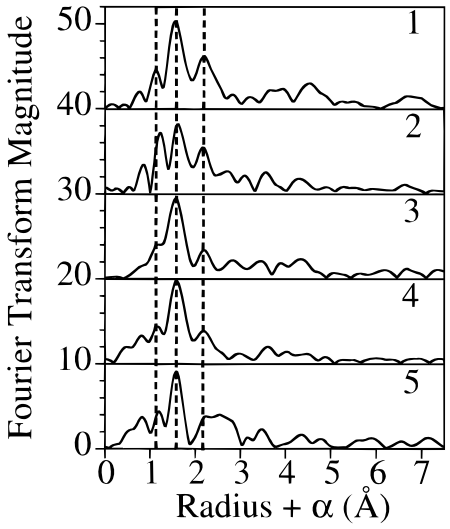

Figure 3. Fourier transforms of the EXAFS data for WT preloaded samples of **X**, samples 1−5. Vertical dashed lines mark the three interactions of interest at 1.8, 2.1, and 2.5 Å.

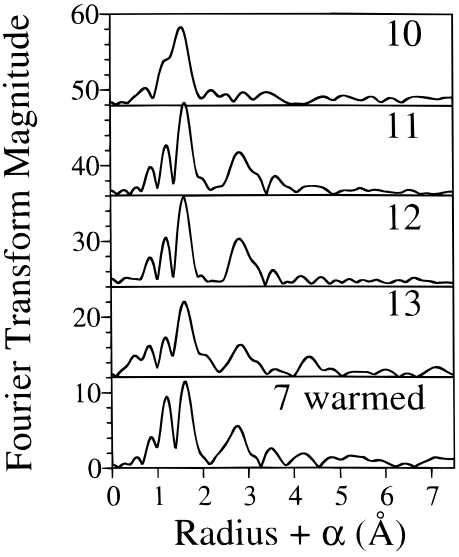

Figure 4. Fourier transforms of the EXAFS data for control samples: sample 10 = WT diferrous R2; sample 11 = WT diferric R2 as isolated; sample 12 = Y122F diferric R2 as isolated; sample 13 = WT-R2 RFQ sample at 1 min (78% diferric R2); sample 7 (Y122F apo reconstituted **X**) warmed to room temperature.

presence of metal back-scattering, since the maximum of the amplitude envelope occurs at a high k value of ∼8 $Å^{-1}$.[62] Figure 3 shows the Fourier transforms (FTs) of the EXAFS spectra of the five individual WT **X** samples (1−5, Table 1). The FTs of all the WT **X** samples have three main interactions that correspond to scatterers at 1.8, 2.1, and 2.5 Å (denoted by vertical lines in Figure 3; note that the abscissa of a Fourier transform is $R + \alpha$, where α is typically −0.4 Å).

For comparison, Figure 4 shows the FTs of the diferrous and diferric (WT and Y122F) controls (10−12, Table 1). The only feature in the FT of RFQ diferrous R2 sample is assigned to the first coordination sphere. The FTs of the WT and Y122F diferric controls have the expected features for a short Fe−O interaction from the μ-oxo bridge and for the Fe−Fe vector at 3.23 and 3.22 Å (samples 11 and 12, respectively). Neither the diferric nor the diferrous controls have a 2.5 Å interaction.

(62) Cramer, S. P.; Hodgson, K. O. In *Progress in Inorganic Chemistry*; Lippard, S. J., Ed.; John Wiley and Sons, Inc.: New York, 1979; Vol. 1−39.

Table 2. Quantitative Fitting Analysis to Fourier-Filtered Data for Preload WT Sample 4 (Table 1) Containing **X**

			O[b]			O/N			C			C			Fe			fit quality	
filter[a]	fit no.	fit category	N[c]	R (Å)	σ^2 [d]	N	R (Å)	σ^2	N	R (Å)	σ^2	N	R (Å)	σ^2	N	R (Å)	σ^2	F	ϵ'
short	4.A	O				3	2.03	5.5										0.545	0.063
	4.B	O, O	1	1.78	6.9	4	2.03	6.4										0.349	0.045
long	4.C	O,O	1	1.79	7.7	4	2.03	6.7										0.682	0.058
	4.D	O, Fe (2.6)[e]				3	2.03	5.6							0.5	2.49	2.9	0.493	0.030
	4.E	O, C (2.6)				4	2.03	8.3	2	2.52	1.0							0.590	0.044
	4.F	O, O, Fe (2.6)	1	1.78	6.2	4	2.03	6.6							0.5	2.49	2.7	0.257	0.011
	4.G	O, O, Fe (2.9)	1	1.79	7.6	4	2.03	6.6							0.5	2.85	3.7	0.570	0.054
	4.H	O, O, C (2.6)	1	1.81	8.5	4	2.04	6.4	2	2.52	0.6							0.358	0.021
	4.I	O, C, C				3	2.03	5.3	2	2.52	0.6	4	2.86	13				0.444	0.033
	4.J	O, C, Fe (2.6)				3	2.03	5.6	2	2.82	12				0.5	2.50	2.8	0.431	0.031
	4.K	O, O, Fe, C	1	1.82	9.8	3	2.04	4.5	3	2.82	8.1				1	2.51	6.7	0.189	0.009

[a] Sample 4 k range = 1.5−12 Å^{-1}; short-filter back transform range = 1.0−2.0 Å, N_{PTS} = 6.7; long-filter back transform range = 0.9−2.7 Å; N_{PTS} = 12.0. [b] Each column represents a shell of scatterers. [c] N = coordination number. [d] σ^2 is in units Å^2 × 10^3. [e] Number in parentheses is the initial Fe−scatterer distance in fit.

Figure 4 also shows the FTs of samples that have been aged (sample 13, containing 78% diferric, 10% **X**, and 10% diferrous and sample 7 after warming). These samples look quite similar to the diferric controls and have no significant intensity at 2.5 Å in the FT. These controls thus suggest that the peak associated with the 2.5 Å interaction is uniquely associated with **X**.

Table 2 gives the results of the curve fitting analyses for WT preload sample 4 which contains ∼58% **X** (Table 1) (results for the WT samples 1, 2, 3 and 5 are given in the supporting material). The feature at 2.5 Å is best modeled with an Fe−Fe interaction at 2.49 Å. Use of a carbon shell at 2.5 Å results in a worse quality of fit (compare fits D and E; compare fits F and H). If the Fe−Fe shell is set initially to 2.9 Å in the fits, the Fe−Fe distance refines to an alternate minimum at ∼2.8 Å, though these fits are considerably worse (compare fits F and G). A comparison of ϵ' values (a fitting statistic that scales the goodness of fit by the number of variables used in the fit) for fits C and F and for fits E and J (Table 2) indicates that addition of the Fe shell significantly improves the fit. In general, the best two and three shell fits contain Fe at 2.5 Å.[63] Figure 5 compares various three shell fits for sample 4. The top frame visually demonstrates that including a short oxo shell, and Fe at 2.49 Å results in the highest quality fit.

Is the 2.5 Å Feature Present in Y122F−R2? Since many spectroscopic studies of R2 cofactor assembly have been carried out on Y122F−R2,[14,15,22] we have examined the EXAFS spectra of Y122F **X** generated from apo-Y122F−R2 (samples 7−9, Table 1) and, in analogy to the WT samples, with preloaded Y122F−R2 (sample 6, Table 1). Figure 6 shows the Fourier transforms of the four samples of **X** prepared from mutant protein. All four samples have a prominent feature at 2.5 Å. Table 3 summarizes curve fitting results to the preload Y122F sample. This sample is similar to the WT preload samples, fitting best with a 2.49 Å Fe−Fe vector. Fits 6.F and 6.J (Table 3), which contain Fe at 2.5 Å, are the best three shell fits. Fits with iron at 2.9 Å (Fit 6.G) or carbon at 2.5 Å (Fits 6.H and 6.I) are worse in quality.

Though Figure 6 clearly indicates that samples of **X** generated from apo-Y122F have a 2.5 Å feature, it cannot be consistently modeled *either* with Fe or with a low Z ligand such as carbon, making an interpretation more difficult. Figure 2C shows the raw EXAFS data for a typical Y122F apo reconstituted sample (sample 7, Table 1), and Table 4 summarizes the fitting results

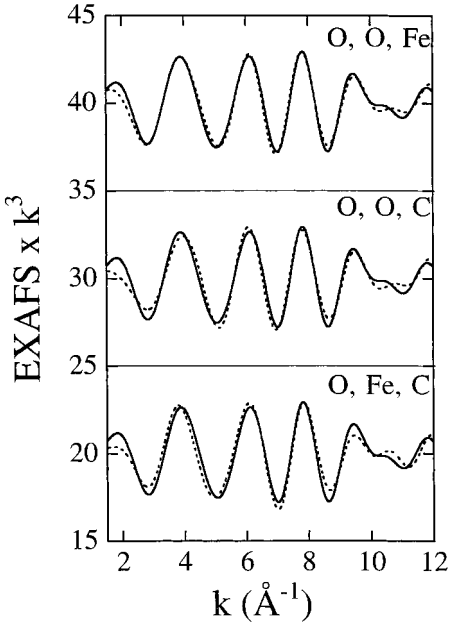

Figure 5. Best three shell fits to the Fourier-filtered data of sample 4 (Table 2): top frame = fit 4.F; middle frame = fit 4.H; bottom frame = fit 4.J; data = solid line, fits = dashed line.

for sample 9 (fitting results for samples 7 and 8 are found in the Supporting Information). For samples 7 and 9, the alternate minimum for the Fe−Fe vector at 2.9 Å is equivalent to or better than the minimum at 2.5 Å (see fits 9.F and 9.G). In samples 7 and 8, the peak at 2.5 Å can be fit equally well with Fe or C at 2.5 Å. Despite the fact that the three apo samples have the same prominent peak at 2.5 Å assigned to an Fe−Fe interaction, when generated under preload conditions, a consistent fitting minimum cannot be obtained.

Another difference between the preload and the apo samples is the behavior of the fits as the parameter ΔE_0 is systematically varied. E_0 is a crucial parameter since its value defines the start of the EXAFS, i.e., the threshold energy where the ejected photoelectron has zero kinetic energy. However, since the value of E_0 cannot be experimentally determined, an initial value is somewhat arbitrarily assigned and the fitting programs allow for adjustments in this assignment with the parameter ΔE_0. In models with isolated metal−metal vectors, a plot of F value vs ΔE_0 for the metal shell has a predictable shape,[64] giving rise to a minimum in F for values of ΔE_0 within a small range (4−14

(63) Four shell fits (i.e., O, O, Fe (2.6), C (2.8) vs O, O, C, C) also show this trend, but ϵ' values for these fits indicate only slight or no improvement in fit relative to the three shell fit (O, O, Fe (2.6)).

(64) Riggs-Gelasco, P. J.; Gelasco, A.; Wright, D.; Armstrong, W.; Pecoraro, V.; Penner-Hahn, J. E. Manuscript in preparation.

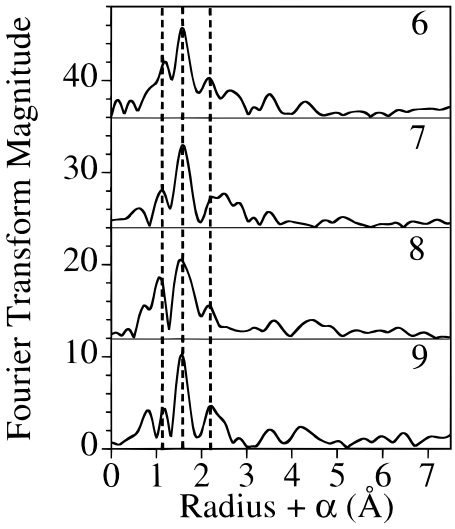

Figure 6. Fourier transforms of the EXAFS data for Y122F samples of **X**. Sample 6 is preloaded whereas samples 7−9 are apo reconstitutions.

eV for the theoretical parameters used in this study[52,53]). If, however, a carbon *shell* is in the vicinity of a metal−metal vector, then the optimal value of ΔE_0 may be offset from this normal range.[54,64] Thus, plots of F vs ΔE_0 have been used to define the metal environment[54,64] and may shed light on the complexities associated with modeling the apo-Y122F **X** data. The top panels in Figure 7 show such plots for the diferric control sample and a WT **X** sample (samples 11 and 4, Table 1). All preloaded samples have this expected shape for the plot of F value vs ΔE_0, indicating that the Fe−Fe vector is relatively isolated from a shell of interfering scatterers. In contrast, the same plots for the Y122F apo samples are aberrant from the normal "U" shape, as demonstrated by sample 9 in the bottom frame of Figure 7. Thus, the inability to resolve consistent minima in the fits to apo-Y122F **X** samples may be due to the presence of additional scatterers near 2.5 Å that obscure the Fe−Fe vector.

The Number of 2.5 Å Scatterers in X. As a dinuclear Fe cluster, **X** is expected to have a single Fe−Fe interaction. For a sample with 50% **X**, the expected number of Fe−Fe interactions would therefore be 0.5, since only half of the Fe in the sample has a detectable Fe−Fe vector. If the 2.5 Å interaction is fit with Fe, the refined number of Fe scatterers ranges from 0.3 to 0.5.[65] If the interaction is modeled with carbon, the optimal number of scatterers is 2−3 *per iron* (Tables 2−4). Since there are no EXAFS observable Fe−C interactions at 2.5 Å in either diferrous or diferric R2, this refined number of 2−3 carbons would imply the existence of four to six new Fe−C interactions at 2.5 Å in **X** *per Fe*, a premise that is unlikely given the available structural data.[4,26,27]

First Shell Interactions. It is clear from the spectroscopic[22,55,60,66] and crystallographic[27] data that during assembly of the diferric cluster, a μ-oxo bridge is generated with a short Fe−O distance (Scheme 1). It is likely that a similar bridge will be present in **X**, given that oxygen from O_2 gas is present in **X**[15] and that the μ-O bridge in the diferric cluster is derived from O_2 gas.[22] All samples of **X** can in fact be fit with a short Fe−O interaction (∼1.8 Å) and a longer (∼2.0 Å) O/N interaction. The former distance is most likely a μ-oxo bridging interaction in **X**, given that most of the samples contain <10% of diferric cluster (Table 1). The latter distance is the weighted average of the longer Fe−O/N distances from carboxylate and histidine ligands in **X** and in the contaminating diferrous and diferric species. The requirement for this short Fe−O interaction to model the first shell data is most apparent when just the first shell is filtered and back-transformed (fits A and B, which are labeled short filters, in Tables 2−4; typical filter range ≈ 1−2 Å). The fit quality improves by an average of 29% for the nine samples of **X** when two Fe−O/N interactions are included (compare ϵ' values for fits A and B, Tables 2−4). When the back-transform filter is extended to include the putative Fe shell and other scatterers beyond 2.5 Å (fits C−K, which are labeled long filters in Tables 2−4; typical filter range ≈ 1−3 Å), the clean resolution of the short μ-oxo shell is partially obscured. An average improvement of 33% is seen when a short oxo shell is added (F fits, Tables 2−4) to the two shell fit containing only O/N and Fe (D fits, Tables 2−4). However, in six of the samples, this three shell fit is not unique; an alternate three shell fit which includes a low Z ligand (carbon) at ∼2.8 Å instead of a short oxo shell also models the data. This ambiguity in the three shell fits most likely indicates that additional scatterers at 2.8 Å (from carboxylate and histidine ligands, for example) contribute significantly to the overall EXAFS signal. Still, in three samples of **X** (2, 4, and 8), the three shell fit containing a short (<1.8 Å, fit category F) oxygen is *significantly* better than the three shell fit without a short interaction (O, Fe, C, fit category J), indicating that **X** does contain a short oxygen ligand.

Control Experiments. To verify that the Fe−Fe interaction at 2.5 Å is not an artifact of the sample geometry, the XAS spectra of diferric (WT and Y122F) and diferrous WT-R2 were collected in the same dual Mössbauer/EXAFS sample cup. As indicated by Figure 4, there is no significant FT intensity at 2.5 Å in samples 10−12 (the diferrous and diferric controls), ruling out any Fe^0 contamination from the cryostat environment as contributing to the peak at 2.5 Å in **X**. We also considered whether freezing into liquid isopentane introduces unanticipated artifacts in the EXAFS. The EXAFS of the freeze-quenched diferrous R2 and the EXAFS of a nonfreeze-quenched diferrous R2 (data not shown)[67] were identical, ruling out structural changes resulting from the freeze quench process. Also, a freeze-quenched sample that was 78% diferric R2 (sample 13) was generated for comparison to the WT diferric sample that was frozen in liquid nitrogen. As shown in Figure 4, sample 13 has the expected 3.2 Å Fe−Fe interaction of the diferric R2 and no significant intensity at 2.5 Å. Finally, sample 7 was allowed to warm to room temperature to demonstrate the conversion of **X** and the 2.5 Å Fe−Fe vector to diferric cluster. Figure 4 shows the FT of sample 7 warmed and the expected appearance of a longer Fe−Fe vector.

While the EXAFS of WT diferric R2 has been published, the EXAFS of Y122F diferric R2 and the EXAFS of diferrous R2 have not been previously reported. The fitting results to these reduced and oxidized control samples are given in the Supporting Information (Tables S.7 and S.8). The fitting results to the diferric WT sample are identical to the most recently reported low-temperature EXAFS of WT-R2, requiring a 3.23 Å Fe−Fe vector and 1.80 Å Fe−O interactions to fit the observed data.[55,60] These same interactions are also required to fit the Y122F data; however, the μ-O interaction in mutant R2 is 1.77 Å, 0.03 Å shorter than the interaction in the WT

(65) Sample 5 can be modeled with two different Fe−Fe vectors (0.3 Fe at 2.52 Å and 0.4 Fe at 2.74 Å, data not shown). The FT of this sample reflects this inhomogeneity (Figure 3).

(66) Bunker, G.; Petersson, L.; Sjöberg, B. M.; Sahlin, M.; Chance, M.; Chance, B.; Ehrenberg, A. *Biochemistry* **1987**, *26*, 4708−47016.

(67) Que, L., Jr. Unpublished results.

Table 3. Quantitative Fitting Analysis to Fourier-Filtered Data for Preload Y122F Sample 6 (Table 1) Containing **X**

			O[b]			O/N			C			C			Fe			fit quality	
filter[a]	fit no.	fit category	N[c]	R (Å)	σ^2 [d]	N	R (Å)	σ^2	N	R (Å)	σ^2	N	R (Å)	σ^2	N	R (Å)	σ^2	F	ϵ'
short	6.A	O				4	2.04	8.8										0.510	0.046
	6.B	O, O	0.5	1.77	1.2	5	2.03	10										0.360	0.036
long	6.C	O, O	1	1.85	9.2	4	2.05	7.2										0.824	0.047
	6.D	O, Fe				4	2.04	9.2							0.5	2.49	2.2	0.646	0.029
	6.E	O, C				5	2.04	11	3	2.51	2.1							0.717	0.036
	6.F	O, O, Fe (2.6)[e]	0.5	1.78	0.8	5	2.03	11							0.5	2.49	2.2	0.535	0.023
	6.G	O, O, Fe (2.9)	1	1.84	8.6	4	2.05	6.9							0.5	2.77	2.5	0.824	0.055
	6.H	O, O, C (2.6)	1	1.84	8.1	5	2.05	8.8	3	2.51	1.9							0.640	0.033
	6.I	O, C, C				5	2.04	11	3	2.52	2.4	2	2.76	1.0				0.619	0.031
	6.J	O, Fe, C				4	2.04	9.6	3	2.76	1.6				1	2.51	5.6	0.562	0.026
	6.K	O, O, C, Fe	1	1.83	6.4	4	2.05	6.4	2	2.75	0.7				0.5	2.51	1.5	0.487	0.023

[a] Sample 6 k range = 1−13 Å^{-1}; short-filter back transform range = 1.0−2.0 Å, N_{PTS} = 7.6; long-filter back transform range = 0.6−3.0 Å, N_{PTS} = 18.3. [b] Each column represents a shell of scatterers. [c] N = coordination number. [d] σ^2 is in units Å^2 × 10^3. [e] Number in parentheses is the initial Fe−scatterer distance in fit.

Table 4. Quantitative Fitting Analysis to Fourier Filtered Data for Apo Y122F Sample 9 (Table 1) Containing X.

			O[b]			O/N			C			C			Fe			fit quality	
filter[a]	fit no.	fit category	N[c]	R (Å)	σ^2 [d]	N	R (Å)	σ^2	N	R (Å)	σ^2	N	R (Å)	σ^2	N	R (Å)	σ^2	F	ϵ'
short	9.A	O				2	2.04	2.7										0.386	0.030
	9.B	O, O	0.5	1.74	0.9	4	2.04	8.8										0.226	0.017
long	9.C	O, O	0.5	1.73	0.8	4	2.03	9.4										0.619	0.045
	9.D	O, Fe				4	2.05	10							0.5	2.49	4.3	0.623	0.045
	9.E	O, C				3	2.05	5.9	2	2.52	0.9							0.618	0.044
	9.F	O, O, Fe (2.6)[e]	0.5	1.74	0.9	4	2.04	8.8							0.5	2.49	3.5	0.405	0.025
	9.G	O, O, Fe (2.9)	1	1.76	7.7	4	2.04	7.6							0.5	2.82	1.7	0.399	0.024
	9.H	O, O, C (2.6)	1	1.74	4.6	5	2.04	10	2	2.51	1.2							0.477	0.034
	9.I	O, C, C				3	2.05	5.9	2	2.54	2.2	3	2.83	3.1				0.421	0.027
	9.J	O, C, Fe				2	2.05	2.6	3	2.81	3.0				0.5	2.52	2.9	0.326	0.016
	9.K	O, O, C, Fe	0.5	1.74	0.6	4	2.04	9.8	2	2.82	1.8				0.5	2.50	4.9	0.221	0.011

[a] Sample 9 k range = 1−12 Å^{-1}; short-filter back transform range = 1.0−2.0 Å, N_{PTS} = 7.0; long-filter back transform range = 1.0−2.8 Å, N_{PTS} = 12.6. [b] Each column represents a shell of scatterers. [c] N = coordination number. [d] σ^2 is in units Å^2 × 10^3. [e] Number in parentheses is the initial Fe−scatterer distance in fit.

sample (fits 11.B and 12.B, Table S.7 of the Supporting Information). The refined Fe−Fe distance is 3.22 Å.

For the reduced sample, the filtered first shell data can only be fit with a single shell of four oxygen/nitrogen ligands at 2.04 Å (fit 10.A, Table S.7 of the Supporting Information). The use of a second shell (fit 10.B, Table S.7 of the Supporting Information) cannot be justified since the ϵ' value does not improve with its use and since the two shells refine to an unrealistic resolution of 0.07 Å.[68] The 3.9 Å Fe−Fe interaction predicted by the crystal structure[26] is too weak to be detected in the EXAFS spectrum of reduced R2.

Table S.8 in the Supporting Information summarizes the fitting results for the aged diferric samples. Short Fe−O interactions are required to fit the first shells of both sample 7 warmed and sample 13, though the Fe−O distance is slightly longer than in the ferric controls (1.83 Å vs 1.80 or 1.77 Å). The second shell of sample 13 is best modeled with an Fe−Fe interaction at 3.24 Å. Sample 7 warmed also has a feature at 3.2 Å, but unlike the other diferric samples, two shells of carbon best model this feature, indicative of some structural damage from the warming process.[69] Despite the fact that neither of these aged samples are 100% diferric R2, and are therefore not ideal controls, Figure 4 and Table S.8 of the Supporting Information indicate that both a 3.2 Å feature and short μ-oxo

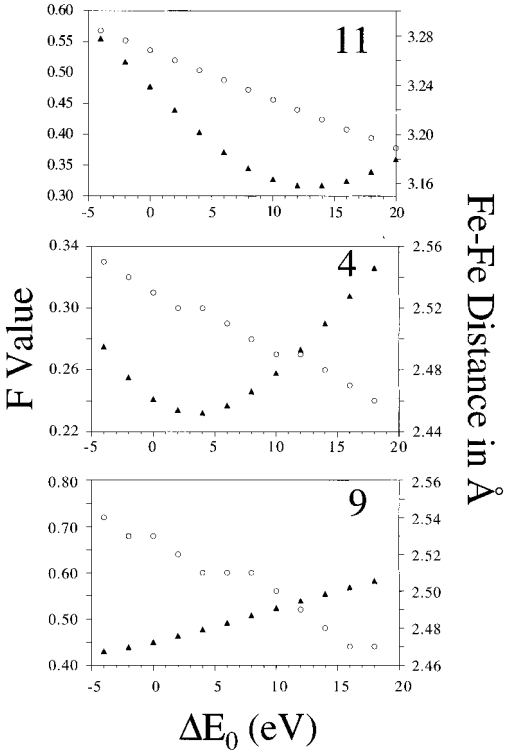

Figure 7. Effect of systematically varying ΔE_0 on F value (triangles) and Fe−Fe distance (open circles), and ΔE_0 was kept fixed at 10 eV in the two oxygen shells: top panel = sample 11; middle panel = sample 4; bottom panel = sample 9.

(68) Resolution can be estimated by the equation $\pi/2\Delta k$, which for this set of data is 0.14 Å.

(69) The evaporation of the isopentane from the sample during the warming process caused sample decomposition as evidenced by severe sample foaming during several attempts to measure this control. Also, warming of metalloproteins after exposure to intense synchrotron radiation often results in sample reduction or degradation. This has occurred to some extent after sample 7 was warmed, as evidenced by a 0.5 eV edge shift to lower energy relative to the diferric controls. Thus, although this control demonstrates the disappearance of the 2.5 Å peak as **X** decays and the appearance of a 3.2 Å interaction as diferric protein is formed, the EXAFS analysis of this sample is not identical to the pure diferric protein.

Table 5. Summary of Distances Obtained for the Nine Samples of **X**[a] and the Five Control Samples[b]

protein	sample	oxo shell distance	O/N distance	Fe−Fe distance
preload WT **X**	1	1.74	2.04	2.49
	2	1.83	2.06	2.49
	3	1.74	2.04	2.49
	4	1.78	2.03	2.49
	5	1.75	2.03	2.49
preload Y122F **X**	6	1.78	2.03	2.49
apo-Y122F **X**	7	1.75	2.04	2.47
	8	1.71	2.00	2.46
	9	1.74	2.04	2.49
diferrous WT	10		2.04	
diferric WT	11	1.80	2.03	3.23
diferric Y122F	12	1.77	2.02	3.22
aged WT (RFQ)	13	1.83	2.05	3.24
aged Y122F (warmed)	7w	1.83	2.04	3.20

[a] For samples of **X**, results from the fits of the type O, O, Fe (fit category F) are reported. [b] For control samples, O, O fits to the first shell are reported; Fe distances result from fits to the second shell of filtered data.

Fe−O distances are present. More importantly, the 2.5 Å peak is significantly reduced in these control samples.

Discussion

A 2.5 Å Feature Is Unique to X. The EXAFS of **X** has been examined in an effort to determine if it possesses a short Fe−Fe distance, an observation that, in conjunction with other spectroscopic methods, would markedly limit its structural possibilities. In this study, nine independently prepared samples with significant amounts of intermediate (53−68%) have a 2.5 Å interaction. The fitting results for these nine samples are summarized in Table 5. This short interaction has been observed using two different beamlines, cryostats, and sample holders and using four different reaction conditions (WT-R2 preload assembly with and without ascorbate, Y122F−R2 preload assembly, and Y122F−R2 apo reconstitution). The interaction does not appear in a RFQ sample containing 92% diferrous R2; it also does not appear in the spectrum of as isolated diferric R2 when measured in the same dual-use sample cup. These controls not only provide reference spectra for these components of the heterogeneous samples but also rule out sample preparation and sample geometry artifacts as the source of the 2.5 Å feature. In addition, a sample containing only 10% **X** and a sample of **X** warmed to room temperature have no detectable 2.5 Å interactions, demonstrating that this feature is unique to samples with significant amounts of intermediate. For the preloaded samples of either WT or Y122F−R2, this 2.5 Å interaction, as discussed subsequently, can be unambiguously assigned to an Fe−Fe vector, a conclusion that will play a key role in the assignment of a structure to **X**.

Interpretation of the 2.5 Å Feature in Preload X. The availability of a di-μ-oxo-bridged compound (**1**), with similar spectroscopic properties to **X**, prompted the EXAFS study of this intermediate in R2 diferric cluster assembly.[37,38] If present in **X**, two single-atom bridges would be expected to afford a prominent Fe−Fe vector in the EXAFS, even in a heterogeneous sample. A number of precedents for EXAFS detectable short metal−metal interactions are apparent from the literature: Mn−Mn vectors of 2.7 Å have been reported for Mn(μ-O)$_2$Mn model complexes and proteins,[54,70−73] Fe−Fe vectors of 2.7 Å have been detected in Fe−S clusters,[74] and a Cu−Cu interaction of 2.5 Å has been detected in the Cu$_A$ center of cytochrome oxidase.[75,76] For samples of **X** generated from the reaction of O_2 with diferrous R2 (samples 1−6), the best two, three, and four shell fits include Fe at 2.5 Å. When the *F* values for the fit category (O, O, Fe) are compared to those from the category (O, O, C), the Fe model is better by an average of 21%. In addition, the refinement of 0.3−0.5 Fe scatterers is within experimental error of the expected number of 0.5 (for a sample with 50% **X**).[77] In contrast, the coordination number for carbon at 2.5 Å is too high to be a valid structural alternative. The refined carbon coordination number indicates each Fe in **X** would have 4−6 new carbon interactions at 2.5 Å. This is an unlikely possibility given that each Fe in **X** has a histidine and an oxo interaction and that the remainder of the carboxylate or water ligands cannot give rise to 4−6 new Fe−C interactions per Fe. The large number of Fe−C interactions necessary to model the 2.5 Å feature most likely reflects the expected trend that ∼6 weakly scattering carbons are required to model the EXAFS of the single Fe−Fe interaction.[78] Further evidence for this is the unusually small σ^2 values obtained for a carbon shell at 2.5 Å.

Apo Reconstitutions. Though it is unlikely that six Fe−C/O interactions from carboxylate ligands form an ordered shell at 2.5 Å, Figure 8 shows that carboxylate ligation (especially bidentate) *could* give rise to Fe−O/C interactions at 2.5 Å.[4,33,55,60,79−84] One or two of these short 2.5 Å Fe−C/O interactions may interfere with the detection of the 2.5 Å Fe−Fe interaction, e.g., for the samples of **X** reconstituted from apo-Y122F. The observations of alternate minima for the metal−metal vector, of 2.5 Å carbon fits that are equivalent or better in quality than the corresponding Fe fits, and of atypical plots of *F* vs ΔE_0 indicate that a metal−metal vector is being obscured by carbon density for these samples.[54,58,85,86] The presence of such interference may be responsible for the decreased precision (compared to the excellent precision for the preloaded samples)

(70) DeRose, V. J.; Mukerji, I.; Latimer, M. J.; Yachandra, V. K.; Sauer, K.; Klein, M. P. *J. Am. Chem. Soc.* **1994**, *116*, 5239−5249.

(71) Penner-Hahn, J. E. In *Manganese Redox Enzymes*; Pecoraro, V. L., Ed.; VCH Publishers: New York, 1992; Vols. 29−46.

(72) Waldo, G. S.; Yu, S.; Penner, H. J. E. *J. Am. Chem. Soc.* **1992**, *114*, 5869−5870.

(73) Yachandra, V. K.; Sauer, K.; Klein, M. P. *Chem. Rev.* **1996**, *96*, 2927−2950.

(74) Teo, B.-K.; Shulman, R. G. In *Iron−Sulfur Proteins*; Spiro, T., Ed.; John Wiley and Sons: New York, 1982; Vols. 343−366.

(75) Blackburn, N. J.; Barr, M. E.; Woodruff, W. H.; van der Ooost, J.; de Vries, S. *Biochemistry* **1994**, *33*, 10401−10407.

(76) Iwata, S.; Ostermeier, C.; Ludwig, B.; Michel, H. *Nature* **1995**, *376*, 660−669.

(77) If the EXAFS spectrum of $[Fe^{3+}(O)_2Fe^{4+}(5\text{-}Me_3\text{-}TPA)]_2](ClO_4)_3$ with its prominent 2.89 Å Fe−Fe vector was added to the EXAFS spectrum of diferrous R2 in a 50:50 mixture, the Fe−Fe peak is dampened by ∼50%, as expected. This calculation also illustrates that an observed 2.5 Å Fe−Fe vector is not artificially generated when the EXAFS of diferrous R2 and a compound with a longer Fe−Fe vector are averaged.

(78) As an example of this, note that six carbons can model the 3.2 Å Fe−Fe vector in diferric R2 (fits 11.C and 11.D, Table S.7 of the Supporting Information).

(79) Nordlund, P.; Åberg, A.; Uhlin, U.; Eklund, H. *Biochem. Soc. Trans* **1993**, *21*, 735−738.

(80) Armstrong, W. H.; Spool, A.; Papaefthymiou, G. C.; Frankel, R. B.; Lippard, S. J. *J. Am. Chem. Soc.* **1984**, *106*, 3653−3667.

(81) Hartman, J. R.; Rardin, R. L.; Chaudhuri, P.; Pohl, K.; Wieghardt, K.; Nuber, B.; Weiss, J.; Papaefthymiou, G. C.; Frankel, R. B.; Lippard, S. J. *J. Am. Chem. Soc.* **1987**, *109*, 7387−7396.

(82) Tolman, W. B.; Liu, S.; Bentsen, J. G.; Lippard, S. J. *J. Am. Chem. Soc.* **1991**, *113*, 152−164.

(83) Rardin, R. L.; Tolman, W. B.; Lippard, S. J. *New J. Chem.* **1991**, *15*, 417−430.

(84) DeWitt, J. G.; Bentsen, J. G.; Rosenzweig, A. C.; Hedman, B.; Green, J.; Pilkington, S.; Papaefthymiou, G. C.; Dalton, H.; Hodgson, K. O.; Lippard, S. J. *J. Am. Chem. Soc.* **1991**, *113*, 9219.

(85) Hedman, B.; Co, M. S.; Armstrong, W. H.; Hodgson, K. O.; Lippard, S. J. *Inorg. Chem.* **1986**, *25*, 3708−3711.

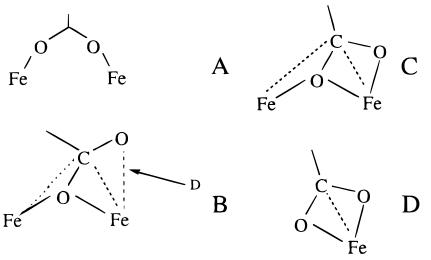

Figure 8. Types of carboxylate ligation with examples from the literature: (A) Bidentate carboxylate bridging. Fe−C vectors ranging from 2.9 to 3.2 Å which are not expected to mimic an Fe−Fe vector at 2.5 Å;[4,79−82] (B) Monodentate carboxylate bridging. For an Fe complex, the Fe−C distances are 2.77−3.17 Å.[82,83] In a recent review, Rardin et al. classified divalent metal complexes with monodentate bridging carboxylates by the extent of interaction between the "dangling" oxygen and the interacting metal.[83] Depending on the strength of this interaction, the distance between the dangling O and the interacting metal ranges from 2.0 to 3.0 Å with virtually every intermediate distance. Such an interaction could contribute to the 2.5 Å feature. However, it is doubtful that this interaction would be EXAFS observable, since such nonbonded interactions are generally not rigid enough to provide significant backscattering intensity. (C) Bidentate chelating, monodentate bridging. In the limit of greatest metal-dangling oxygen interaction, the oxygen becomes a ligand and the bridging mode becomes bidentate chelating, monodentate bridging. Glu243 in reduced soluble methane monooxygenase from *Methylococcus capsulatus* (Bath) adopts this bridging mode where the distance from Fe2 to the δ-C is 2.64 Å.[33] However, this interaction is not observable in the EXAFS of reduced MMO.[84] (D) Bidentate chelating carboxylate. Fe−C distances could be in the range of 2.5 Å. In diferric R2, the carboxylate carbon from the bidentate ligation of Asp-84 is 2.7 Å away from the chelated Fe.[4] This distance could be shorter with higher oxidation state. This short Fe−C interaction was not detectable in the protein EXAFS diferric R2.[55,60]

in the Fe−Fe distance determination for the Y122 apo reconstituted samples of **X**, as Table 5 summarizes.

While it is reasonable that the lack of a definitive Fe−Fe vector in the apo reconstituted samples arises from overlap with Fe−C vectors, we do not know the source of this interference. Several possibilities have been considered, and the present data do not allow us to distinguish between them. For example, the increased interference could indicate a subtle change in the mechanism of carboxylate shifts which result in Fe−C interactions overlapping with the Fe−Fe vector. This rationale is supported by kinetic differences between the apo reconstituted and the preload samples of **X**.[87] However, Mössbauer and ENDOR spectra of **X** indicate no detectable structural differences when **X** is generated from WT or Y122F or from preload or apo reconstitutions.[14] It should also be noted that the preload and apo reconstitutions differ in the time that **X** optimally accumulates. Recent ^{17}O ENDOR spectra suggest that a terminal water bound to **X** exchanges with solvent during assembly, indicating that time dependent changes in the structure of **X** are occurring.[25] Future experiments will address the very subtle differences in structure noted in this study.

Oxo Bridging in X. The presence of the 0.5−1.0 Fe−O interactions at 1.8 Å strongly implicates the presence of at least one oxo bridge in **X**. The Fe−O distance in a hydroxyl bridge would be longer[88] than the observed 1.77 Å and is similarly ruled out by recent proton ENDOR experiments.[24] When the first shell alone is filtered and back-transformed, an improvement in fit is apparent when an oxo shell is included (see fits A and B, Tables 2−4). When the back-transform is over a wider range, the oxo shell can also be uniquely refined in three data sets, providing evidence for the presence of μ-oxo bridging in **X**. For the remaining samples, two different three shell fits (either fit category F or J, Tables 2−4) can model the observed data. The short Fe−O distance is difficult to detect in the presence of the Fe and C shells. Despite these difficulties in refining the shorter Fe−O shell, the EXAFS can be conservatively interpreted as providing evidence for at least one μ-oxo bridge in **X**. These results are consistent with the ^{17}O ENDOR studies of **X** assembled with $^{17}O_2$ gas which suggest the presence of a single ^{17}O atom in a bridge.[25]

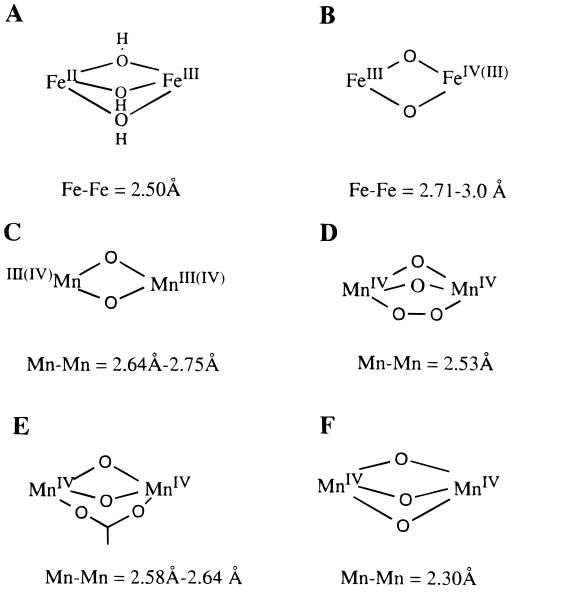

Figure 9. Examples of synthetic model complexes with short metal−metal distances. (A) $[L_2Fe^{II}/Fe^{III}(\mu\text{-}OH)_3][BPh_4]_2\cdot 2MeOH$ where L = *N*,*N*′,*N*″-trimethyl-1,4,7-triazacyclononane.[89,90] (B) $[Fe^{3+}(\mu\text{-}O)_2Fe^{4+}(5\text{-}Me_3\text{-}TPA)]_2(ClO_4)_3$ where 5-Me$_3$-TPA = tris(5-methyl-2-pyridylmethyl)amine;[37] $[Fe^{III}_2(O)_2(6\text{-}Me_3\text{-}TPA)_2](ClO_4)_2$ where 6-Me$_3$-TPA = tris(6-ethylpyridyl-2-methyl)amine;[36] $[Fe^{III}(O)_2(6\text{-}Me\text{-}TPA)]_2Fe^{IV}]$.[91] (C) Examples include $[Mn^{IV}(salpn)O]_2$ where salpn = *N*,*N*′-bis(salicylimino)propanediamine;[92,93] di-μ-oxotetrakis(2,2′-bipyridine)dimanganese-(III,IV).[94] (D) $[L_2Mn^{IV}_2(\mu\text{-}O)_2(\mu\text{-}O_2)](ClO_4)_2$ where L = 1,4,7-triazacyclononane.[95] (E) $[L(Mn^{III}(\mu\text{-}O)_2(CH_3COO)Mn^{IV}L]$ where L = 1,4,7-triazacyclononane;[96] $[Mn^{IV}_2(\mu\text{-}O)_2(O_2CCH_3)(H_2O)_2(bpy)_2](ClO_4)_3$ where bpy = 2,2′-bipyridine;[97] $[Mn_2(\mu\text{-}O)_2(O_2CCH_3)(tpen)](ClO_4)_2$ where tpen = *N*,*N*,*N*′,*N*′-tetrakis(2-pyridylmethyl)-1,2-ethanediamine.[98] (F) $[LMn^{IV}(\mu\text{-}O)_3Mn^{IV}L](PF_6)_2\cdot H_2O$ where L = *N*,*N*′,*N*″-trimethyl-1,4,7-triazacyclononane.[99]

Structural Possibilities for X. The experiments, when compared to the controls, suggest that a novel 2.5 Å feature is present in samples containing significant amounts of **X** (>50%). This feature is not observed in diferrous or diferric R2 and is not observed in samples where **X** has decayed. In addition, a short Fe−O distance which is most likely a μ-O interaction has been detected. When **X** is generated starting with diferrous R2, the 2.5 Å feature is unambiguously modeled with ∼0.5 Fe at 2.49 Å. From crystallographically characterized model compounds (Figure 9) it is known that the presence of three bridges is required to achieve a M−M interaction as short as 2.5 Å. Many of the model compounds contain two μ-oxo bridges in addition to a third bridge. However, three hydroxyl bridges also result in a short interaction,[89,90] suggesting that other models with three single atom bridges may also result in a short Fe−Fe vector.

(86) Scott, R. A.; Eidsness, M. K. *Comments Inorg. Chem.* **1988**, *7*, 235−267.

(87) Tong, W.-H.; Burdi, D.; Riggs-Gelasco, P.; Chen, S.; Han, S.; Edmondson, D. E.; Huynh, B. H.; Tainer, J.; Stubbe, J. Submitted to *Biochemistry*.

(88) Zang, Y.; Pan, G.; Que, L., Jr.; Fox, B. G.; Münck, E. *J. Am. Chem. Soc.* **1994**, *116*, 3653−3654.

While this work was in progress, Shu et al. also discovered a 2.46 Å Fe−Fe interaction in an EXAFS study of intermediate **Q** in MMO.[43] The authors assigned the structure of **Q** to be an asymmetric di-μ-oxo-bridged core, with a third bridge from a bidentate carboxylate ligand. This asymmetric diamond core was proposed on the basis of the observation of 1.77 and 2.05 Å Fe−O/N interactions and a larger area for the 1s → 3d transition for **Q** relative to diferrous MMO. In our study of intermediate **X**, we have observed similar interactions. However, the average 2.03 Å Fe−O/N interaction observed in our samples cannot be assigned uniquely to a structural feature in **X**, since the 50% diferrous R2 contaminant has prominent EXAFS interactions at 2.04 Å (Table 5). Several possible core structures for **X** have been considered (Figure 10) that satisfy the structural constraints imposed by our EXAFS results and the crystallographic data on diferrous and diferric R2.[4,26,27] Structures A and B include a bidentate carboxylate bridge, a feature which may not allow a short enough Fe−Fe distance. However, in the absence of suitable models and given that Glu115 is bidentate and bridging in both diferrous and diferric R2, we have included these as possible structures. Structures A and C in Figure 10 have di-μ-oxo-bridged cores, with structure A being the motif that Shu et. al chose to explain the 2.46 Å interaction in **Q**. Structure D is equally attractive with three single atom bridges deriving from an oxo bridge and two monodentate bridging carboxylates. A similar option cannot be ruled out for **Q** in MMO, given the available data. We currently favor structure D for the core of **X** on the basis of ^{17}O ENDOR experiments that have traced the fate of the oxygen atoms in the activating $^{17}O_2$ gas. One of the oxygens is assigned to a terminal bound water which exchanges with solvent; the second is associated with the μ-oxo bridge.[25] Together, the EXAFS and ENDOR RFQ studies suggest that D (Figure 10) is the best model at present for **X**.

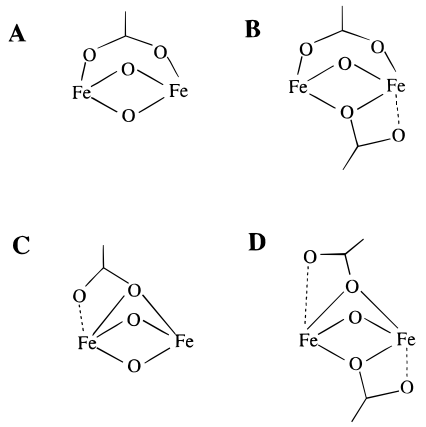

Figure 10. Possible protein core structures that could account for the observed short Fe−O distance and the 2.5 Å Fe−Fe interaction. Dashed lines on carboxylate bridges could be bonding (bidentate chelating) or nonbonding interactions.

Acknowledgment. This research is supported in part by grants from the National Institutes of Health (GM29595 to J.S., F32 GM17963 to P.R.-G. and GM47295 to B. H. H.), the National Science Foundation (MCB-9405723 to L. Q.), the University of Minnesota Graduate School (Doctoral Dissertation Fellowship to L. S.), and the American Cancer Society (postdoctoral fellowship to D. B.). NSLS and SSRL are supported by the US Department of Energy with additional support from the NIH Research Resource program. The authors thank Prof. Stephen Lippard for providing the coordinates for the reduced MMO structure and Xuedong Wang for helping with data collection. The authors also thank Dr. Wing Tong, Prof. James Penner-Hahn, Prof. Brian Hoffman, and Dr. Britt Hedman for helpful discussions. We also thank members of the SSRL biotechnology group for assistance with data collection, especially Paola de Cecco.

Supporting Information Available: Results to fitting analyses for samples **1**−**3**, **5**, **7**, **8**, **10**−**13** and **7w**, a summary of fitting results using the FABM method of analysis, and the dimensions of the dual Mössbauer/EXAFS sample cell (10 pages). See any current masthead page for ordering and Internet access instructions.

JA9718230

(89) Drüeke, S.; Chaudhuri, P.; Pohl, K.; Wieghardt, K.; Ding, X.-Q.; Bill, E.; Sawaryn, A.; Trautwein, A. X.; Winkler, H.; Gurman, S. J. *J. Chem. Soc., Chem. Commun.* **1989**, 59−62.

(90) Gamelin, D. R.; Bominaar, E. L.; Kirk, M. L.; Wieghardt, K.; Solomon, E. I. *J. Am. Chem. Soc.* **1996**, *118*, 8085−8097.

(91) Shu, L.; Dong, Y.; Que, L., Jr. Unpublished results.

(92) Gohdes, J. W.; Armstrong, W. H. *Inorg. Chem.* **1992**, *31*, 368−373.

(93) Larson, E. J.; Pecoraro, V. L. *J. Am. Chem. Soc.* **1991**, *113*, 3810−3818.

(94) Plaskin, P. M.; Stoufer, R. C.; Mathew, M.; Palemik, G. J. *J. Am. Chem. Soc.* **1972**, *94*, 2121.

(95) Bossek, U.; Weyhermüller, K.; Wieghardt, K.; Nuber, B.; Weiss, J. *J. Am. Chem. Soc.* **1990**, *112*, 6387.

(96) Haselhorst, G.; Wieghardt, K. *J. Inorg. Biochem.* **1995**, *59*, 624.

(97) Pal, S.; K., C. M.; Armstrong, W. H. *J. Am. Chem. Soc.* **1992**, *114*, 6398−6406.

(98) Dave, B. C.; Czernuszewicz, R. S.; Bond, M. R.; Carrano, C. J. *Inorg. Chem.* **1993**, *32*, 3593−3594.

(99) Wieghardt, K.; Bossek, U.; Nuber, B.; Weiss, J.; Bonvoisin, J.; Corbella, M.; Vitols, S. E.; Girerd, J. J. *J. Am. Chem. Soc.* **1988**, *110*, 7398−7411.